Acta Oceanol. Sin., 2018, Vol. 37, No. 1, P. 20–29
DOI: 10.1007/s13131-018-1155-y
http://www.hyxb.org.cn
E-mail: hyxbe@263.net

The spring Yellow Sea fog: synoptic and air–sea characteristics associated with different airflow paths

HUANG Jian[1], WANG Bin[2], WANG Xin[3], HUANG Fei[4], LÜ Weihua[1], Tu Jing[1]*

[1] Institute of Tropical and Marine Meteorology, China Meteorological Administration, Guangzhou 510080, China

[2] Department of Meteorology, University of Hawaii, Honolulu HI 96822, USA

[3] South China Sea Institute of Oceanology, Chinese Academy of Sciences, Guangzhou 510301, China

[4] Physical Oceanography Laboratory, Ocean University of China, Qingdao 266100, China

Received 18 July 2016; accepted 17 January 2017

Abstract

The fog occurs frequently over the Yellow Sea in spring (April–May), a climatical period of Asian monsoon transition. A comprehensive survey of the characteristic weather pattern and the air-sea condition is provided associated with the fog for the period of 1960–2006. The sea fog is categorized by airflow pathways of backward trajectory cluster analysis with the surface observations derived from international comprehensive ocean-atmosphere dataset (I_COADS) I_COADS datasets and contemporaneous wind fields from the National Centers for Environmental Prediction (NCEP)/National Center for Atmospheric Research (NCAR) reanalysis. On the basis of the airflow paths, the large-scale lower-tropospheric circulation patterns and the associated surface divergence, the distribution of a vertical humidity, the horizontal water vapor transportation and the air-sea temperature difference are investigated and the major findings are summarized as follows. (1) Four primary clusters of the airflow paths that lead to spring sea fog formation are identified. They are originated from the northwest, east, southeast and southwest of the Yellow Sea, respectively. (2) Springtime Yellow Sea fog occurs under two typical weather patterns: the Yellow Sea high (YSH) and cyclone and anticyclone couplet (CAC). Each pattern appears by about equal chance in April but the YSH occurrence drops to around one third and the CAC rises to around two third of chance in May. (3) The common feature in the two types of synoptic conditions is that surface divergence center is located over the Yellow Sea. (4) For the YSH type of fog, water vapor comes mainly from local evaporation with a well-defined dry layer present in the lower atmosphere; for the CAC type of fog, however, water vapor comes mainly from areas outside the Yellow Sea with a thick surface layer of high humidity. (5) With the differences in weather patterns and its associated vertical distribution of the humidity and the transportation of water vapor, there are two types of sea fogs. Most fogs of the CAC types are “warm” fog, while fogs of YSH type have nearly equal chance to be “warm” and “cold” fog.

Key words: springtime sea fog, Yellow Sea, airflow clusters, synoptic patterns, characteristics of sea fog

Citation: Huang Jian, Wang Bin, Wang Xin, Huang Fei, Lü Weihua, Tu Jing. 2018. The spring Yellow Sea fog: synoptic and air–sea characteristics associated with different airflow paths. Acta Oceanologica Sinica, 37(1): 20–29, doi: 10.1007/s13131-018-1155-y

1 Introduction

Among China’s offshore waters, the Yellow Sea fog is characterized by the huge coverage, long time of occurrence, extended duration of the fog season, and significant seasonal variations. Reducing both horizontal and vertical visibility over the sea and coasts, sea fog severely affects all kinds of sea-based activity, including marine fishing, rig drilling, commercial shipping, military operations, airplane flights and highway travel, and is one of the main causes for serious accidents.

It is widely accepted that most of the Yellow Sea fog is resulted from the cooling of air due to the advection of a warm and humid airflow over a cold sea surface, while some of it is generated from frontal surfaces (Wang, 1985; Zhou and Liu, 1986). As the principal reason, the sea fog forms when sea currents with relatively cool sea surface temperature (SST) are heading north along the coast and meet relatively warm and moist airflows that are transported from the Sea of Japan and the Northwest Pacific (Wang, 1985). In addition, the cold-water pool due to upwelling or the turbulent mixing induced by strong tide currents are the major causes for the frequent occurrence of the sea fog (Wang, 1985; Zhou and Liu, 1986; Cho et al., 2000).

In fact, the Yellow Sea fog is unique. It can be formed in various weather systems, originated from mid-latitude associated winter monsoon, or from tropics and subtropics associated with summer monsoon (Zhou et al., 2004; Wang et al., 2006), including the high pressure that moved out of continent, intrusion of the ridge of the North Pacific High, and the low or trough migrated from the China’s Mainland into the Yellow Sea (Wang, 1985). As such, the sea fog must be formed with different meteorological and marine environment. Some previous works have shown that water vapor associated with the Yellow Sea fog formation has different origins in the fog season (Zhou et al., 2004;

Foundation item: The National Natural Science Foundation of China under contract No. 41275025; the Special Fund for Strategic Pilot Technology of Chinese Academy of Sciences under contract No. XDA11010403; the National Key Basic Research Program (973 Progrom) of China under controut No. 2014CB953903.
*Corresponding author, E-mail: 375834995@qq.com

Huang and Zhou, 2006). Little has been known of the meteorological and marine characteristics of the Yellow Sea fog under different synoptic conditions, particularly the different physical mechanisms for the sea fog development and persistence under the control of winter and summer monsoons. Recently, it is suggested that the sea fog over the Yellow Sea shows a seasonal variation representing monsoon characteristics, especially in boreal spring of Asian monsoon transition period from winter monsoon to summer monsoon (Zhang et al., 2009). However, it is still not clear whether the sea fog over the Yellow Sea in spring is a warm fog or cold fog during the sea fog development and persistence (Zhang and Ren, 2010), and what the marine meteorological conditions in favor of warm and cold fog formation, development, persistence and dissipation are.

In the marine environment, the exchange of heat and water vapor with the sea surface during the advection of air mass is particularly important to the fog formation and persistence (Wang, 1985; Koračin et al., 2005, 2014). For this reason, tracing the pathways of the airflow is an objective and efficient mean to study the marine and meteorological conditions of the sea fog (Lewis et al., 2003). In this study, we used the method of a backward trajectory analysis and cluster analysis to determine the source regions of the airflows in April and May for the period of 1960–2006. On the basis of the airflow analysis, we analyzed the typical weather patterns for the sea fog occurrence and the vertical distribution of humidity, water vapor transportation and air-sea temperature differences; discussed the commonality and difference in physical processes of the sea fog formation between two synoptic patterns. The aim is to provide a comprehensive survey of the characteristic weather pattern and air-sea condition associated with the fog, and throws some light on forecasting.

2 Data and methodology

2.1 *Data*

The data of fog during the period of 1960–2006 used in this study include the observations from an international comprehensive ocean-atmosphere dataset (I_COADS) compiled by the National Climate Data Center (NCDC) (Woodruff et al., 1987; Bottomley et al., 1990), and contemporaneous NCEP/NCAR reanalysis data, which are available four times daily at 2.5°×2.5° grid points on standard pressure surfaces (Kalnay et al., 1996).

Being the most complete and comprehensive dataset of observations in the world, the I_COADS comprises measurements taken on commercial, military or research vessels, mooring buoys and other types of maritime platforms. The observations are made up of a series of independent texts that report on the wind direction, wind speed, air temperature, the dew point and the weather phenomenon over the sea surface and the SST in every 3 h (Worley et al., 2005). Owing to the marine environment and communication condition, surface reports from the I_COADS are not always believable. In this study, the rigid quality control processes are applied as follows. (1) Only highly reliable records, based on quality control mark of the I_COADS are available. (2) According to ship call letters, observed time, locations and content, the observed data sets are tested one by one. The duplicate reports and wrong reports on land were deleted. (3) The observation reports of the Yellow Sea are tested by climatological means, referring that the variations of oceanic and atmospheric variables are limited in climatic ranges. For example, in this paper, limits for the SST, the air temperature and the sea level pressure are in –2°C to 40°C, –50°C to 50°C, and 950–1 050 hPa, respectively. (4) Finally, the anomalies of these variables are tested to ensure the reliability of the reports. For instance, the air temperature reports are available only if the absolute values of the anomaly are less than 10°C. Detailed technologies for the quality control and data verification are documented by Huang and Zhou (2006).

In this study, fog occurring in the central area of the Yellow Sea (32°–39°N, 121°–126°E) is chosen from I_COADS as this area has the highest observation frequency (Wang et al., 2004). This choice also avoids the effect of a coastal fog such as radiation fog (Huang and Zhou, 2006). In accordance with the specifications of the National Weather Service of USA for the use of the I_COADS, the fog is represented with the codes of 28, 41–47 if visibility is less than 1 km or with the codes of 10 and 12 if visibility is less than 1 km but the height of fog layer is less than 10 m (National Weather Service, 1991). The fully developed fogs (Codes 28, 41–47) have been picked out, and the light fog and shallow fog that are less than 10 m in height (Codes 10–12) were given up. In the central Yellow Sea, there are a total of 1 137 records of sea fog in April and 2 128 in May. In addition, if three or more fog records at different sites are reported at same time, then one sample of fog is identified. According to this threshold, 279 and 387 fog samples are determined in April and May, respectively.

The sea fog appears in the central Yellow Sea (32°–39°N, 121°–126°E) is analyzed in this study because this area has the highest frequency of occurrence, good data coverageand representativeness (Wang et al., 2004). This choice also avoids the effect of coastal fog such as radiation fog on the sample. This study focus on the open sea fog that has fully developed and with considerable thickness (Codes 41–47). The light fog and shallow fog that is less than 10m in height (Codes 10–12) are excluded. There are a total of 1 137 records of sea fog in April over the area of interest and a total of 2 128 in May. In addition, if one of the weather codes appears more than three records, a sample of fog is then defined. Screened against this threshold, 279 and 387 effective fog samples are determined for April and May, respectively. Detailed technologies for the quality control and the data verification are documented in Huang and Zhou (2006) and Huang et al. (2010).

2.2 *Methodology*

In the previous statistical analysis of the Yellow Sea fog, weather situations where sea fog forms are usually determined using the weather map. Since the fog may occur at different locations of a given synoptic system, the circulation, dynamic and thermodynamic structures of the lower atmosphere may have large differences. The sea fogs are predominantly advection fog and the formation of which is closely related to the exchange of heat and water vapor over the sea surface during advection (Wang, 1985). The SST changes are mainly governed by the solar radiation, although meteorological conditions, ocean currents, land-sea distribution and terrain may also affect the SST (Yan et al., 1993). Therefore, the analysis of the air mass displacement and the similar trajectory of the air mass over the sea facilitate the classification of the sea fog, then the sea fog with similar meteorological and marine conditions can be identified. The following steps and methods are used in the analysis.

First, based on the observations of the I_COADS and the wind field data of NCEP/NCAR reanalysis, 36 h backward trajectories are computed for each of the sea fog samples using the backward trajectory analysis for the airflow, which is described mathematically by Draxler (1996) as follows:

$$P(t+\Delta t)=P(t)+0.5[V(P,t)+V'(P',t+\Delta t)]\Delta t,$$
$$P'(t+\Delta t)=P(t)+V(P,t)\Delta t,$$

where $P(t)$ is the location of the trajectory at time t; $V(P, t)$ is the wind speed at time t and point $P(t)$; $V'(t+\Delta t)$ is the location of the trajectory with the elapse of a time step Δt; and $V'(P', t+\Delta t)$ is the wind speed at point $V'(t+\Delta t)$ with the elapse of Δt, determined by interpolation. Because of the relatively coarse resolution for the data set of the NCAR/NCEP and the frequency of fog occurrence (Wang, 1985; Zhao et al., 1997), the location (35°N, 124°E) in the middle of the Yellow Sea, the key area of this study, is assumed to be the starting point of the airflow tracing. Second, the method of cluster analysis, which follows the principle of looking for spatial and temporal closeness in classifying multiple clusters of airflow by degrees of similarity, is used to categorize the background clusters into different groups (Stunder, 1996). Last, based on the grouped airflow clusters and geopotential heights from the reanalysis of the NCEP/NCAR, an empirical orthogonal function (EOF) analysis is used to study the principal modes corresponding to various groups of the airflow clusters. Some marine and meteorological elements and associated parameters are studied by a composite analysis for the same category of trajectory to determine composite fields. The composite fields may represent the common characteristics of the sea fog of each type.

3 Results

3.1 *Typical airflow pathways*

Figure 1 shows the typical airflow clusters associated with the sea fog events obtained from the 36 h backward trajectory and cluster analysis for April and May, respectively. There are four groups of clusters (T-NW, T-E, T-SE and T-SW) for the airflow that eventually result in the fog in April; T-NW is a northwest airflow from the continental area to the North Yellow Sea; T-E is an east airflow from the southern Korean Peninsula; T-SE is a southeast one from the Northeast East China Sea; T-SW is a southwest airflow from the western Yellow Sea waters around 35°N. In addition, the four groups of the airflow clusters also differ in the move speed. It is known from the length of the clusters presented in Fig. 1a that the airflow moves much faster along T-NW and T-SE than that along T-E and T-SW. The flow path in May is similar to that in April, but the T-SW in April is more northward than that in May. It can be inferred from the oceanic and atmospheric thermodynamics as well as the migratory clusters of the airflow in April and May, the sea fog along T-NW is mostly related to a cool and dry air mass moving over warmer water or along cold fronts. While that along T-SW, T-E and T-SE may be mainly caused by advective cooling.

It is worth noting that the percentage of the sea fog occurrence for the four groups differs between April and May (Table 1). For April, the sea fog with the T-NW trajectory has the highest ratio (30.1%), followed by T-SE (27.3%). May is much different from April in that the sea fog is the most frequent with T-SE and T-E; the ratio with the T-NW trajectory substantially drops to 13.7% while that with T-SE is the highest (41.1%) and T-E also increases to 26.6%. The airflow clusters are closely related to the circulation of synoptic regimes. Based on the climate background, although the winter monsoon has weakened and retreated to the north in April, the winter monsoon system remains active over the Yellow Sea; on the other hand, with the onset of the East Asian summer monsoon in May, tropical synoptic systems such as the subtropical high gradually advances northward. It is then concluded that the difference in the airflow trajectories associated with the Yellow Sea fog reflects the changes in the prevailing weather systems as the Yellow Sea experiences transitions from the winter monsoon to the summer monsoon.

3.2 *Synoptic patterns of the Yellow Sea fog*

Synoptic patterns associated with the sea fog indicate weather conditions where the sea fog formed over a particular area of waters, or main weather systems and the allocation among themselves. Usually, the weather maps are used to classify the weather patterns, but it is very complicated and subjective and lack of unified standards. Following the cluster analysis described in Section 2, the 279 sea fog samples in April account for 84, 59, 60 and 76 events of T-NW to T-SW clusters, respectively; the 387 samples in May account for 53, 72, 103 and 159 of T-NW to T-SW clusters, respectively. Here, the geopotential heights of the NCEP/NCAR for different clusters of the sea fog samples were used to investigate the characteristics of the spatial distribution of the major modes of the synoptic patterns, i.e., geopotential height fields, for different clusters of the sea fog by applying the EOF decomposition.

First of all, the variance contribution by the EOF-decomposed first mode in April and May is between 85% and 90% for the four groups of clusters with the 1 000 hPa geopotential heights (Table 2), while more than 90% with the 850 hPa geopotential heights (table omitted). Additionally, the first mode and the distribution of corresponding temporal coefficients shown in Figs 2 and 3 indicate that the latter is positive. Thus, the first mode alone contains most of the information about the geopo-

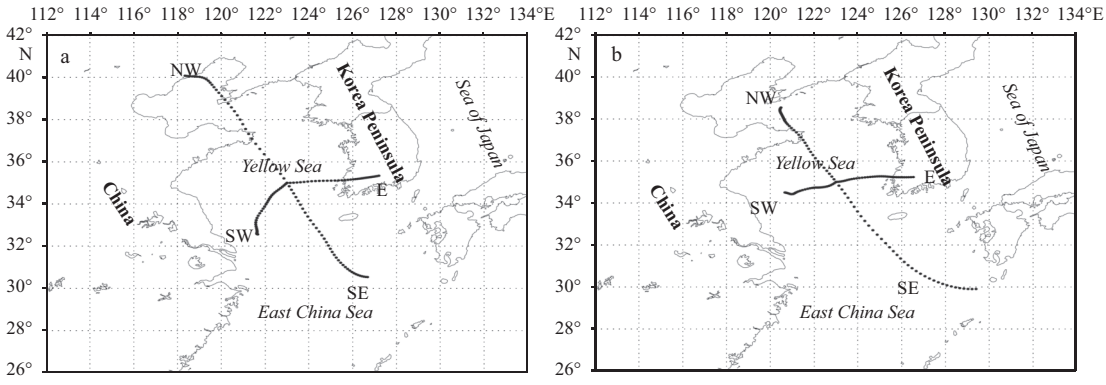

Fig. 1. Mean trajectories of the airflow for the formation of theYellow Sea fog in April (a) and May (b). All trajectories stand for the 36 h backward trajectories.

Table 1. Percentage (%) of the sea fog with the four groups of airflow clusters for the Yellow Sea

	Clusters			
	T-NW	T-SW	T-E	T-SE
April	30.1	21.1	21.5	27.3
May	13.7	18.6	26.6	41.1

Table 2. Variance (%) contribution accounted for the first EOF mode with the 1 000 hPa geopotential heights for the four groups of airflow clusters in April and May

	Clusters			
	T-NW	T-E	T-SE	T-SW
April	89.1	90.4	88.0	87.3
May	84.5	87.9	87.2	87.1

tential height field.

Both originating from the Yellow Sea, T-NW is from the northwest part while T-SW is from the southwest part of the sea Fig. 1). As shown in the primary EOF mode of the 1 000 hPa geopotential heights in April, the Yellow Sea is dominated by an isolated high; but the centers of the high with T-NW (Fig. 2a) is more southward and slightly stronger than that of T-SW (Fig. 2d). The primary EOF mode of the 850 hPa geopotential heights (Figs 3a and d) is nearly the same as in 1 000 hPa. The main trough in East Asia is located near 140°E and the Yellow Sea is located in the high pressure ridge behind the East Asian Trough. Although T-NW and T-SW represent northwest and southwest airflows, respectively, they are associated with the same weather system (high surface pressure). The difference between T-NW and T-SW is only due to the fact that they occur on difference phases of the high pressure system. Both T-NW and T-SW share the same weather pattern, which is named as the Yellow Sea high (YSH).

The airflows along T-E and T-SE originated from the east and southeast, have totally different weather patterns from that of T-NW and T-SW. For T-E, the Yellow Sea is a low pressure region with a high pressure to the east and a low over China's Mainland (Fig. 2b). For T-SE, the Yellow Sea is also located in a low pressure area with a high to the east and a low center over China's Mainland (Fig. 2c). Compared with the trajectory of T-SE, the low pressure associated with T-E is stronger and covers a larger area. Likewise, the 850 hPa circulations associated with T-E and T-SE has little difference; both show that the East Asian Trough is relatively shallow and located between 120°E and 125°E over the Yellow Sea (Figs 3b and c). This pattern is called a cyclone and anticyclone couplet (CAC).

The primary EOF modes in May are nearly the same to the corresponding counterparts in April (Figs 4 and 5). For both T-NW and T-SW the Yellow Sea is under control of a high pressure with a slight difference in the location of the center. In T-NW the Yellow Sea is located to the east of the high and a central pressure is higher while for T-SW the Yellow Sea is located to the west of the high pressure center and the high is weaker. The leading EOF mode for T-SE is also nearly the same that in April. The only difference between April and May is seen in T-E group. The high pressure to the east of the Yellow Sea is enhanced. At 850 hPa, the leading EOFs associated with T-NW and T-SW are nearly identical (Figs 5a and d): the northeast–southwest tiled East Asian Trough is located around 140°E and the Yellow Sea is controlled by a high pressure ridge. Similarly, the leading EOFs associated with T-E and T-SE show a shallow East Asian Trough with trough line located between 120° and 125°E over the Yellow Sea. In summary, two basic weather patterns associated with the Yellow Sea fog have been identified. One is the YSH, and the other is CAC. The former is associated with the northwest and southwest pathways of the air flows, whereas the latter is associated with the east and southeast airflow pathways. This is true for both April and May. The results obtained by the objective EOF analysis are con-

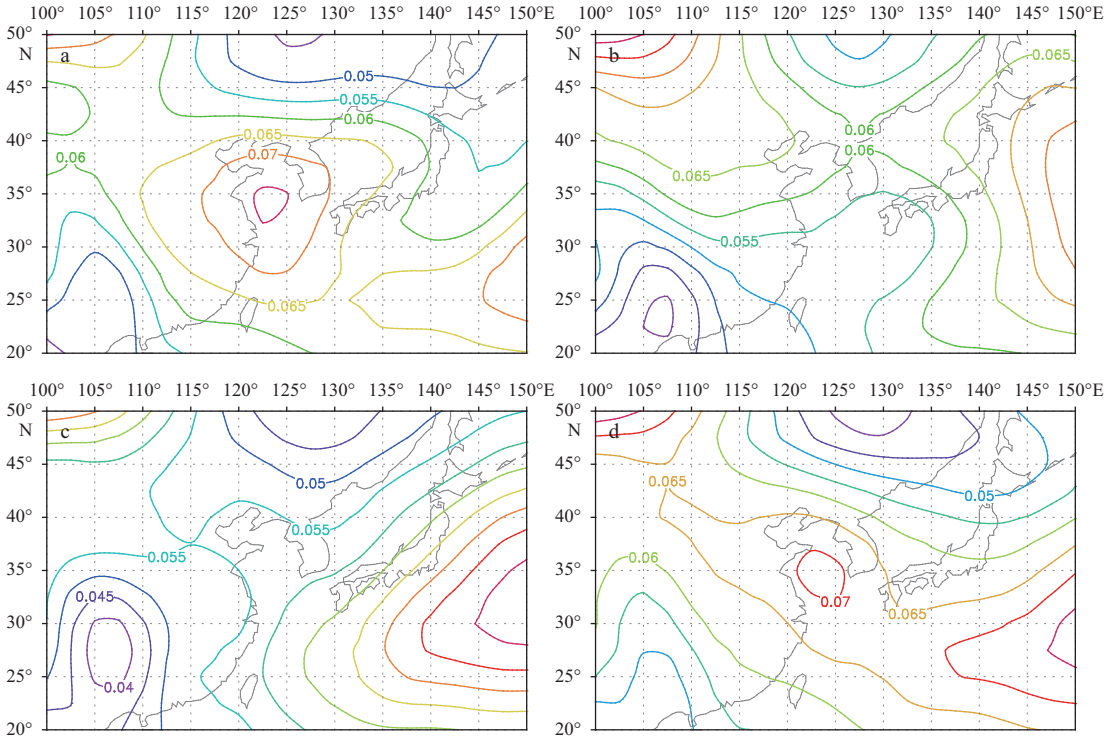

Fig. 2. The first EOF modes of the 1 000 hPa geopotential height for four groups of airflow clusters in April. a, b, c and d correspond to T-NW, T-E, T-SE and T-SW in Fig. 1a, respectively.

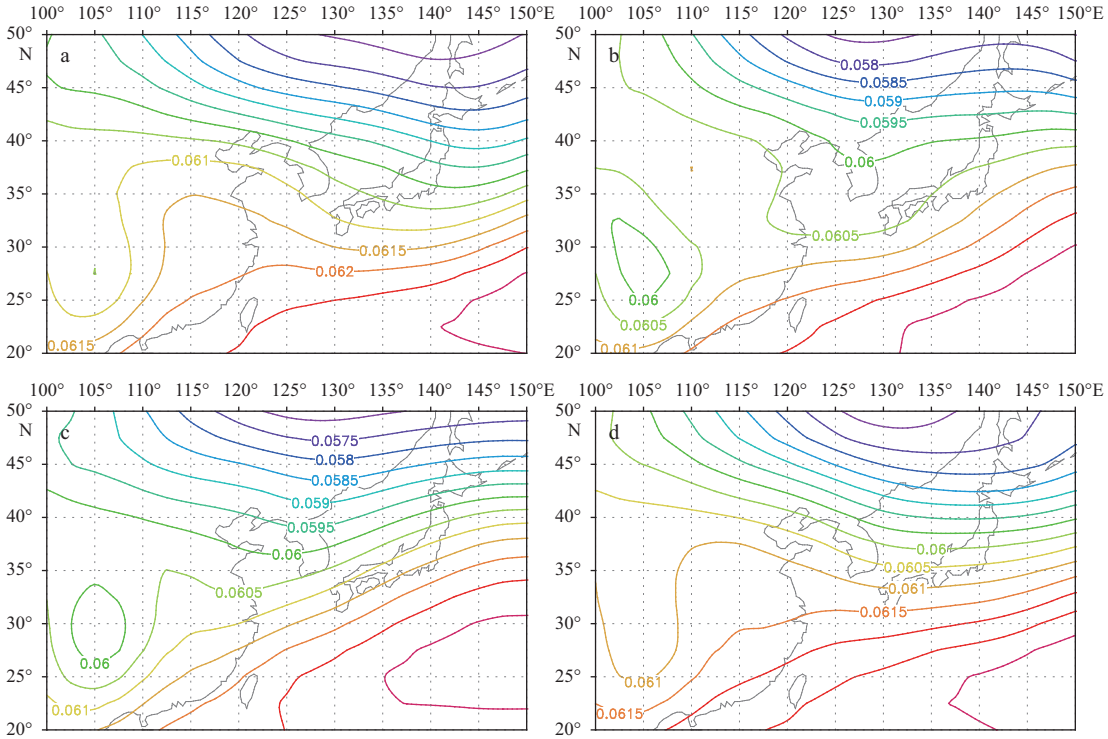

Fig. 3. The first EOF modes of the 850 hPa geopotential height for four groups of airflow clusters in April. a, b, c and d correspond to T-NW, T-E, T-SE and T-SW in Fig. 1a, respectively.

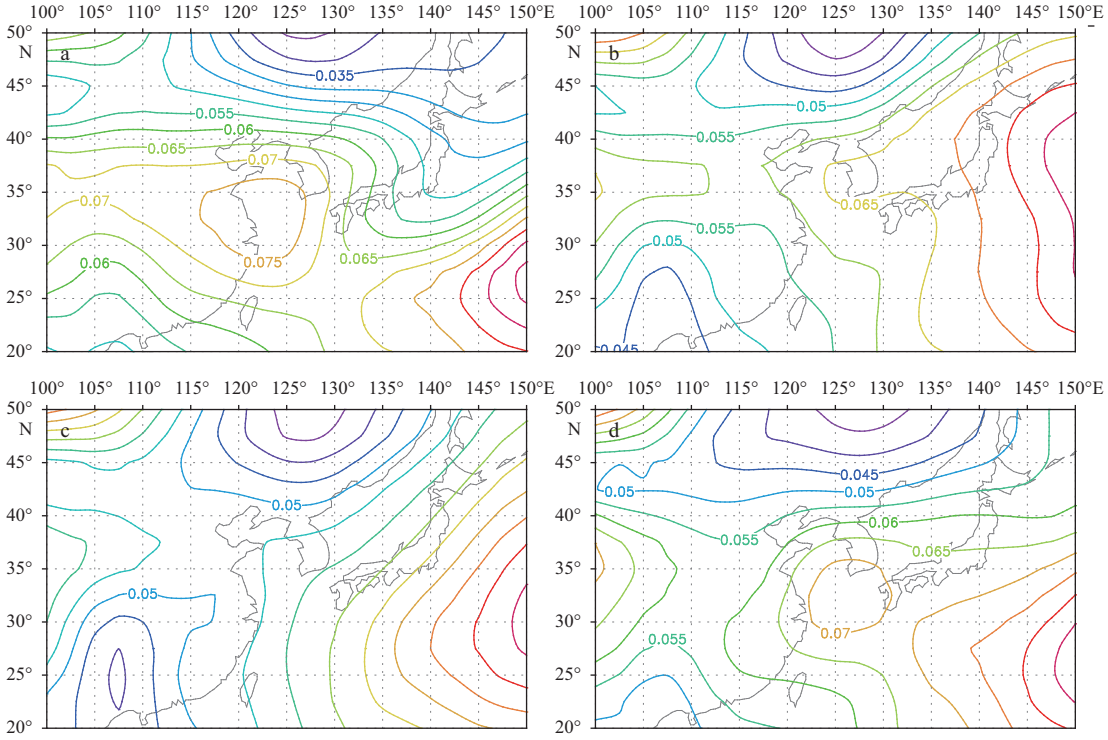

Fig. 4. The first EOF modes of the 1 000 hPa geopotential height for four groups of airflow clusters in May. a, b, c and d corresponds to T-NW, T-E, T-SE and T-SW in Fig. 1b, respectively.

sistent with the previous results obtained by examination of satellite imagery and weather maps (Zhao et al., 1997).

Based on the results shown in Table 1, it is found that during April, the YSH and CAC patterns associated with the sea fog occurs at about equal chance, while in May the YSH occurrence drops to about one third and the CAC rises to about two thirds of chance. An interesting result is that the principal component (PC) of T-NW appears different interannual variabilities compar-

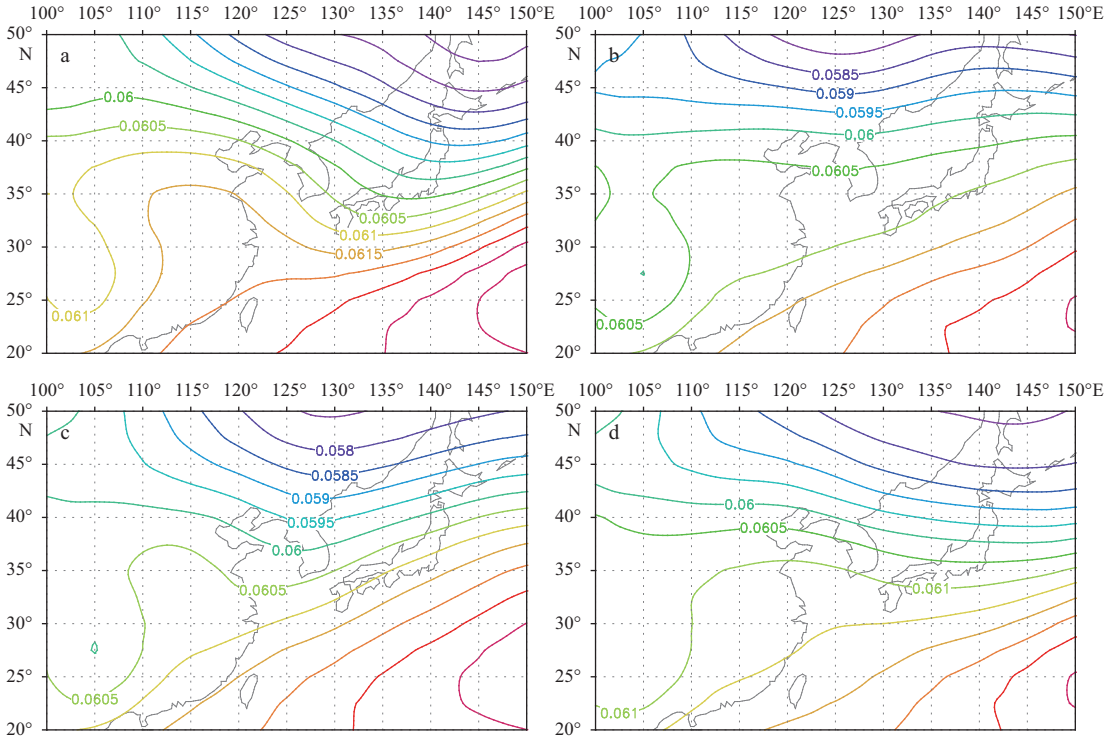

Fig. 5. The first EOF modes of the 850 hPa geopotential height for four groups of airflow clusters in May. a, b, c and d corresponds to T-NW, T-E, T-SE and T-SW in Fig. 1b, respectively.

ing with those of T-E, T-ST and T-SW both in April and May, although T-NW and T-SW have similar spatial patterns. Meanwhile, although the four groups of trajectories in April and May are similar spatial patterns, their PCs show different interannual variations between April and May as well.

3.3 *Characteristics of the surface divergence field*

After examining the connection between fog events along the US west coast and large-scale atmospheric circulation, Filonczuk et al. (1995) suggested that the fog occurrence was not dominated by local processes. Positive 700 hPa height anomalies correspond to subsiding an air and a high occurrence of fog in all regions of the state. Other studies also show that the air subsidence often occurs above inversion in the lower troposphere (Leipper, 1994; Roach, 1995a). Here we use the NCEP/NCAR reanalysis data to compute the divergence field for all sea fog events and then made composited field for four groups of pathways.

Figures 6 and 7 present the 1 000 hPa atmospheric divergence fields corresponding to the four groups of airflow trajectories in April and May, respectively. The most significant characteristics of the divergence field, as shown in Figs 6 and 7, are the presence of independent centers of the divergence for all of the four groups. Similar divergence structure also exists for the fields of various airflows on 850 hPa (figure omitted). AS far as system characteristics are concerned, the two different types of surface pressure pattern in April and May (Figs 2 and 4) are found to have similar structure in the 850 hPa circulation (Figs 3 and 5). Obviously, the divergence fields are dynamically coherent with the circulation pattern. A divergent lower atmosphere in which the air descends dynamically helps dry the upper boundary layer and form stable stratification, which trap the water vapor near the sea surface within a certain altitude (Rogers and Koračin, 1992; Leipper, 1994).

The stable stratification in the course of the spring Yellow Sea fog is generally believed to be caused by advection of warm and humid air over a cool sea surface (Gao et al., 2007). In fact, such phenomenon is not entirely the cause of the advection because dynamic structure in the weather patterns also contributes to the fog formation process. Leipper (1994) also suggested that the exchange of heat between the air and sea tends to make the near-sea-surface air temperature to be consistent with the SST; the existence of the temperature inversion noted at the lower layers of the atmosphere during a sea fog is mainly attributed to the heating effect of the descending air.

During the spring Yellow Sea fog days, the stable stratification of the lower atmosphere has something to do with the warming induced by the descending motion associated with the systems. The divergence fields with the two weather types are so consistent with each other that it is particularly indicative as an important dynamic factor of the lower atmosphere for the sea fog forecasting.

3.4 *Characteristics of vertical distribution of relative humidity*

Compared with the wind, pressure and temperature fields, the humidity field of the NCEP/NCAR reanalysis data is relatively less reliable. But the reanalysis is the only long-term data set available up to the present and it does reflect the characteristics of the large-scale synoptic regimes to some extent.

Figure 8 presents the composite relative humidity profile showing the vertical distribution of the relative humidity along 125°E for the four groups of pathways in April. Over the Yellow Sea (33°–39°N), for the T-NW and T-SW pathways, the high relative humidity occurs near the sea surface, which is accompanied by an extremely dry overlying layer. On the other hand, for the T-E and T-SE pathways the high relative humidity is not only seen near the sea surface but also in a thick layer well above the sea

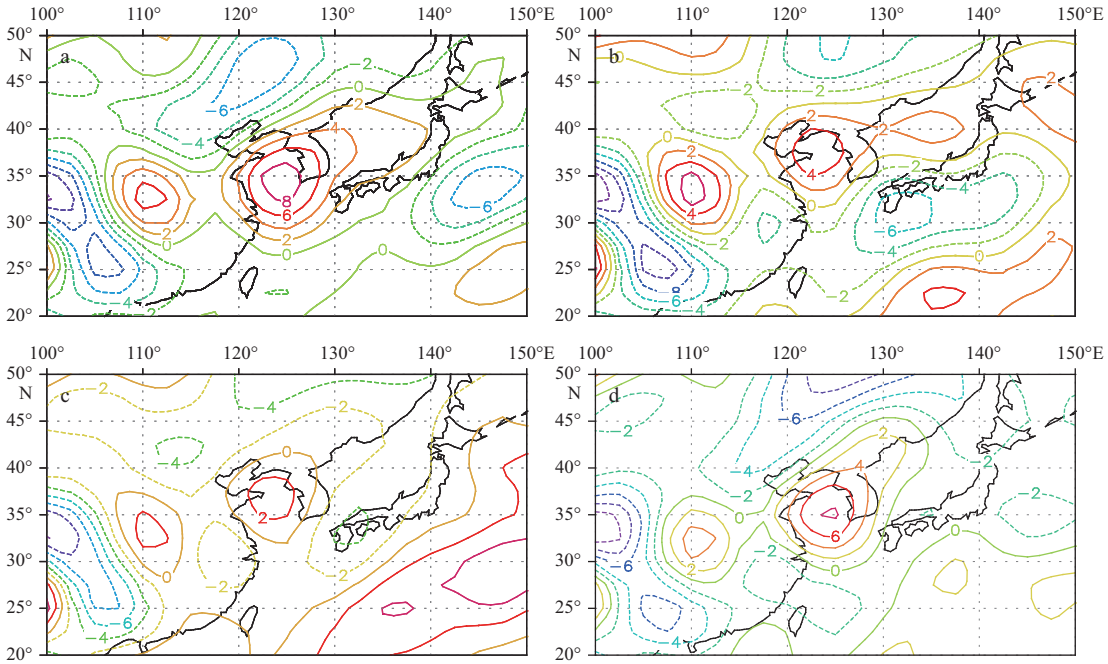

Fig. 6. Divergence (10^{-6} s^{-1}) at 1 000 hPa for the four groups of clusters in April. a. T-NW, b. T-E, c. T-SE and d. T-SW.

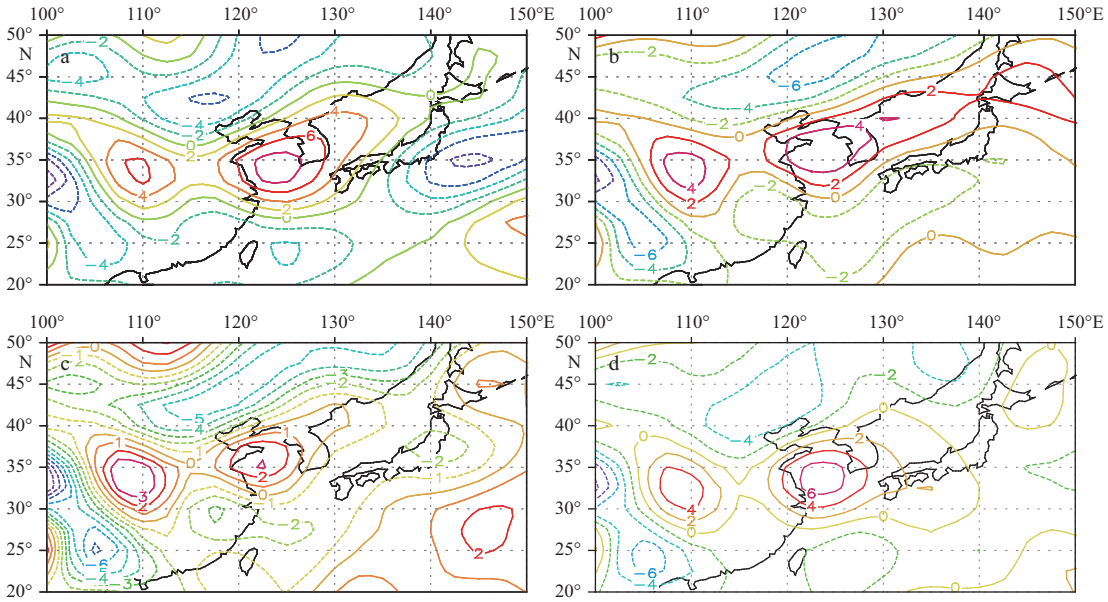

Fig. 7. Divergence (10^{-6} s^{-1}) at 1 000 hPa for the four groups of clusters in May. a. T-NW, b. T-E, c. T-SE and d. T-SW.

surface. The vertical distribution of the relative humidity in May is very similar to that in April (figure omitted).

The vertical distribution of the relative humidity with the four trajectory groups are related to the thermodynamic nature of the weather systems. The dominant weather system with T-NW and T-SW is the YSH, which is originated from a continental cold and dry high pressure over the middle and higher latitudes. In spite of the exchange of heat and vapor over the sea surface during the movement of the high and the consequent rise of the air temperature and the relative humidity in the layer near the sea surface, the stable stratification and subsidence in a high pressure system usually constrain turbulence within a limited altitude so that the air above the moist layer maintains the thermodynamic characteristics of its origin. However, for the T-E and T-SE groups, the Yellow Sea is located between the marine high to the east and the continental low pressure to the west. Influenced by the convective activity embedded in the low pressure system, it is reasonable to have a thick layer of the high relative humidity.

Soon after the thin fog layer forms, the longwave radiative cooling at the fog top takes over the cooling of the development and persistence of the sea fog (Lamb, 1943; Findlater et al., 1989). The efficiency of the long wave radiative cooling depends on the difference between the upward long wave radiation emitted from the fog top and the downward long wave radiation from the atmosphere above the fog top. When dry air overlies the shallow and moist marine layer, there will be less downward inverse radi-

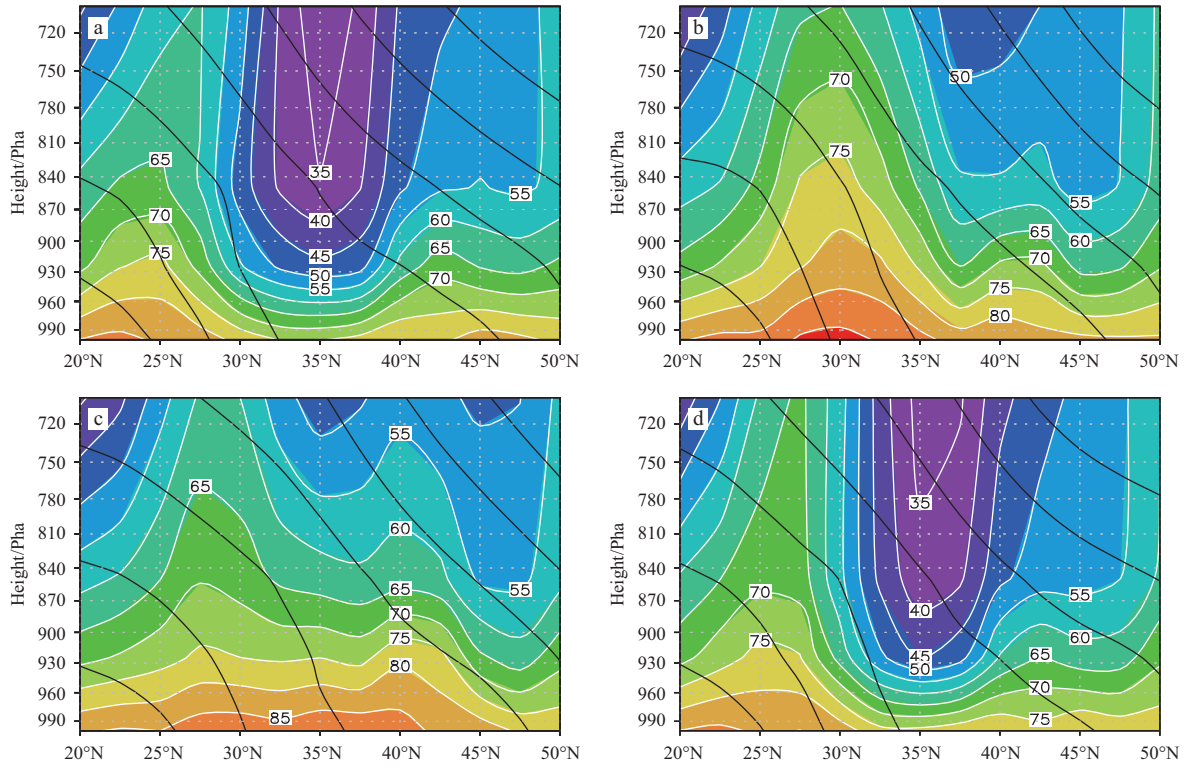

Fig. 8. The vertical distribution of the relative humidity (%) and the temperature along 125°E for four airflows in April. The Yellow Sea is between 33° and 39°N. The white contours stand for the relative humidity and the black contours denote temperature (K). a. T-NW, b. T-E, c. T-SE and d. T-SW.

ation, thus the net long wave radiative cooling will be more effective and vice versa. The two patterns of the relative humidity at lower atmosphere might indicate some difference on the cooling process of the sea fog.

3.5 *Characteristics of water vapor advection*

Fog formation and persistence require a water vapor supply to offset the water vapor lost due to the deposition of fog droplets and to maintain the equilibrium of the water vapor in fog (Roach, 1995b). The main sources of water vapor of the sea fog are advection of moist air and evaporation from both local sea surface and rain droplets descending from higher levels (Wang, 1985).

The horizontal water vapor flux reflects the transportation direction and magnitude of water vapor and its source. With the sea surface wind fields and specific humidity data from the I_COADS, the fluxes of water vapor near the sea surface are individually calculated to examine the transport of the water vapor in fog for the four trajectory groups. The equation used for this purpose is $-\vec{V}q\Delta p$, where $\vec{V}$ is the vector of the horizontal wind, q is the specific humidity and Δp is the difference in the vertical air pressure, which is taken to be 1 hPa in this work. As the water vapor flux is similar between April and May, only the figure for May is given here.

With different sources of water vapor, the water vapor is transported also differs dramatically (Fig. 9). Not much water vapor is transported to the Yellow Sea as the T-NW trajectory is from the northwest (Fig. 9a). Though from areas southwest of the Yellow Sea, water vapor via the T-SW trajectory does not result in much larger transportation, as the airflow is a southwest return airflow at the rear of the YSH (Fig. 9d). Originating from the southeast, the T-SE type of the airflow carries water vapor, by the largest amount of the four pathways, into the Yellow Sea from the East China Sea (Fig. 9c). Coming from Korean Peninsula and the Sea of Japan to the east of the Yellow Sea, the water vapor conveys by T-E trajectory less than by T-SE, but more than T-NW or T-SW (Fig. 9b). As shown in Fig. 8, the relationships between the vertical distribution of the relative humidity and the advection-transported water vapor are so close that strong transportation leads to a relatively thick layer of the relative humidity in the lower atmosphere and vice versa.

With the CAC pressure pattern, water vapor is mainly supplied via advection from waters outside the Yellow Sea, which makes favorable condition for the fog formation. With the YSH pattern, on the other hand, the circulation of the winter monsoon system does play a role in transporting some water vapor to the Yellow Sea but its amount is just too little. To a larger extent, water vapor with the YSH pattern is supplied by local evaporation from the sea surface. According to Zhou et al. (2004) and Huang et al. (2010), water vapor for the spring sea fog in the Yellow Sea does not originate from local sources but is transported from a tropical atmosphere, which is obviously not applicable for the case of the YSH.

3.6 *Air-sea temperature difference*

Taylor (1917) has studied sea fogs near Newfoundland and found that the fog is due to air blowing off warm water on to the cold water of the Banks, but fog temperatures range from several degrees Celisus warmer than the sea to 1–2°C colder than the sea. “Warm” fog tend to occur in warm air advection conditions, while “cold” fogs tend to occur in winds too light to allow kite flying (Taylor, 1917).

The maintenance of the “cold” fog is linked to radiative cool-

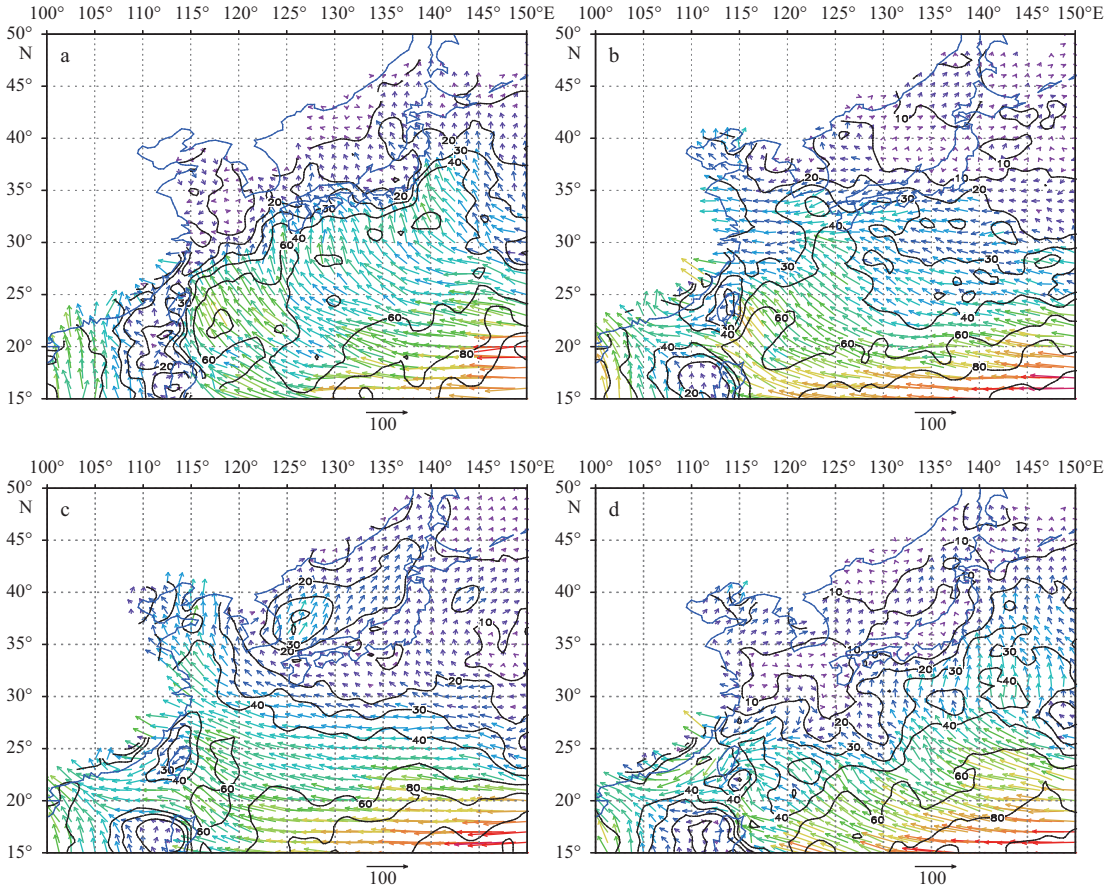

Fig. 9. Horizontal water vapor flux (g/(10⁴·m·hPa·s)) of sea surface for the sea fog over the Yellow Sea in May. a. T-NW, b. T-E, c. T-SE and d. T-SW.

ing at the top of the fog (Douglas, 1930; Lamb, 1943; Findlater et al., 1989). Once the fog is formed, the long wave radiative cooling at its top generates turbulent mixing and the growth of the fog as a mixed layer. Owing to cooling, the fog layer is colder than the underlying surface, the transfer of heat from the sea is warming up the fog layer and offsetting the loss of heat and moistening the air by means of evaporation (Findlater et al., 1989; Koračin et al., 2005). In this case, the long wave radiation plays a particularly important role: whenever clouds appear on top of the fog layer, the fog will be dissipated (Roach, 1995a). In "warm" fog, the physical process for the fog development and persistence becomes more complicated. Various mechanisms are thought to be responsible for, the cooling is a result of combined effects of the turbulent transfer of sensible and latent heats and the radiation from the air to the sea interface as well as long wave radiation (Wang, 1985).

Within the area of interest at the Yellow Sea, there are 1 137 and 2 128 records of the sea fog for April and May, respectively. The air-sea temperature difference in the record was grouped by airflow clusters to obtain percentages of the "warm" fog (in which the air temperature is higher than the sea surface temperature) for each of the clusters (Table 3). For the sea fog with the YSH pattern, the "warm" fogs take up18% with the T-NW cluster in April, including the frontal fog, and increase to 48% in May. For the T-SW cluster, they are 48% and 49% respectively for April and May, which are close to the ratio of T-NW for May. For the "warm" fogs with the CAC pattern, there are 56% and 66% respectively for April and May with the T-E cluster and 68% and 70% with the T-SE cluster respectively for April and May. With the transition of circulation from winter monsoon to summer monsoon, the ratio of positive air-sea temperature differences increases to some extent. It is shown in Sections 3.4 and 3.5 that the YSH pattern is the characteristic of a weak advective transport of water vapor and resultant dry layers at lower atmospheric levels, which implies the presence of favorable conditions for cooling through the long wave radiation at the top of the fog layer. On the other hand, the CAC pattern is marked by significant transportation of water vapor with a relatively thick layer of the high relative humidity, which may reduce the cooling effect of longwave radiation at the fog top. It is then inferred that the cool/warm fogs are in close association with the nature of the accompanying synoptic patterns and its seasonal transition.

Table 3. Statistics of positive temperature differences (%) between the sea and air (air temperature minus sea temperature being equal to or greater than 0) for all groups of airflow clusters

	Cluster			
	T-NW	T-E	T-SE	T-SW
April	18	56	68	45
May	48	66	70	49

4 Conclusions

With the methods of the backward trajectory and the cluster analysis, the airflow pathways have been grouped for the spring Yellow Sea fog. On the basis of this grouping, the EOF technology

has been further used to analyze the weather types (situations) corresponding to the airflow clusters. The synoptic, meteorological and maritime environments have been studied including the dynamic characteristics, vertical distribution of humidity and transportation of water vapor, and the physical properties of the springtime sea fog over the Yellow Sea.

(1) Compared with the previous subjective classification method based on the weather maps, the current approach, based on the clusters of airflow and the objective EOF analysis, better summarizes the synoptic characteristics of the sea fog in detail, and the deduced weather patterns have clearer synoptic implications.

(2) The airflows associated with the spring Yellow Sea fog have four origins: northwest, east, southeast and southwest of the Yellow Sea. In April, the northwest and southwest airflow have greater frequency of occurrence than the east and southeast airflows; in May, things are just on the opposite, indicating the impact of the seasonal transition from the winter monsoon to the summer monsoon.

(3) The weather patterns associated with the spring Yellow Sea fog can be categorized as two basic types: the Yellow Sea high (YSH) and the cyclone and anticyclone couplet (CAC). Each of them takes up about half of the April sea fogs, but the chance of occurrence for the first pattern drops to around one third while the second one rises to about two thirds in May.

(4) For both YSH and CAC patterns, the low troposphere (1 000 hPa and 850 hPa) are marked with well-defined divergence in the fog regions, which is one of the most significant features for two types of sea fog weather patterns.

(5) There is remarkable difference in the distribution of vertical humidity and origin of water vapor between the YSH and CAC patterns. The former has a distinctive dry layer in the lower atmosphere with water vapor mainly originating from local position of the Yellow Sea; the latter has a thick, wet layer with water vapor mainly coming from waters of the west of Japan or the Northwest Pacific, which are all outside of the Yellow Sea.

(6) With the substantial differences in the weather pattern and associated vertical distribution of humidity and transportation of water vapor through advection, the percentage of "warm" fogs ranges from 45–48% in the YSH case while in the range of 56–70% in the CAC case. The result here suggests that the spring Yellow Sea fog forms under two typical weather situations, the processes and mechanisms of sea fog formation are different. This result provides a useful guidance for the numerical modeling and the operational forecast of the sea fog.

References

Bottomley M, Folland C K, Hsiung J, et al. 1990. Global ocean surface temperature atlas (GOSTA). London: UK Depts of Energy and Environment, 303–313

Cho Y K, Kim M O, Kim B C. 2000. Sea fog around the Korean Peninsula. J Appl Meteor, 39(12): 2473–2479

Douglas C. 1930. Cold fogs over the sea. Meteor Mag, 65: 133–135

Draxler R R. 1996. Trajectory optimization for balloon flight planning. Wea Forecasting, 11(1): 111–114

Filonczuk M, Cayan D, Riddle L. 1995. Visibility of marine fog along the California coast. Scripps Institution of Oceanography Report 95–2, 99–102

Findlater J, Roach W T, McHugh B C. 1989. The haar of north-east Scotland. Quart J Roy Meteor Soc, 115(487): 581–608

Gao Shanhong, Lin Hang, Shen Biao, et al. 2007. A heavy sea fog event over the Yellow Sea in March 2005: analysis and numerical modeling. Chinese Advances in Atmospheric Sciences, 24, 65–81

Huang Jian, Wang Xin, Zhou Wen, et al. 2010. The characteristics of sea fog with different airflow over the Yellow Sea in boreal spring. Acta Oceanol Sin, 29(4): 3–12

Huang Jian, Zhou Faxiu. 2006. The cooling and moistening effect on the formation of sea fog in Yellow Sea. Acta Oceanol Sin, 25(2): 49–62

Kalnay E, Kanamitsu M, Kistler R, et al. 1996. The NCEP/NCAR 40-year reanalysis project. Bull Amer Meteor Soc, 77(3): 437–471

Koračin D, Leipper D F, Lewis J M. 2005. Modeling sea fog on the U.S. California coast during a hot spell event. Geofizika, 22: 59–82

Koračin D, Dorman C E, Lewis J M, et al. 2014. Marine fog: a review. Atmos Res, 143: 142–175

Lamb H. 1943. Haars or North Sea Fogs on the Coasts of Great Britain. London: Meteorology Office Publication, 21–24

Leipper D F. 1994. Fog on the U.S. west coast: a review. Bull Amer Meteor Soc, 75(2): 229–240

Lewis J, Koračin D, Rabin R, et al. 2003. Sea fog off the California coast: viewed in the context of transient weather systems. J Geophys Res, 108(D15): 4457, doi: 10.1029/2002JD002833

Lewis J M, Koračin D, Redmond K T. 2004. Sea fog research in the United Kingdom and United States: a historical essay including outlook. Bull Amer Meteor Soc, 82(3): 395–408

National Weather Service. 1991. National Weather Service Observing Handbook (No. 1): Marine Surface Weather Observations. Sliver Spring, Maryland: Untied States Department of Commerce, 102–120

Roach W T. 1995a. Back to basics: fog: Part 3 The formation and dissipation of sea fog. Weather, 50(3): 80–84

Roach W T. 1995b. Back to basics: fog: Part 2 The formation and dissipation of land fog. Weather, 50(1): 7–11

Rogers D P, Koračin D. 1992. Radiative transfer and turbulence in the cloud-topped marine atmospheric boundary layer. J Atmos Sci, 49(16): 1473–1486

Stunder B J B. 1996. An assessment of the quality of forecast trajectories. J Appl Meteor, 35(8): 1319–1331

Taylor G I. 1917. The formation of fog and mist. Quart J Roy Meteor Soc, 43(183): 241–268

Wang Binhua. 1985. Sea Fog (in Chinese). Beijing: China Ocean Press, 323–330

Wang Xin, Huang Fei, Zhou Faxiu. 2006. Climatic characteristics of sea fog formation of the Huanghai Sea in summer. Haiyang Xuebao (in Chinese), 28(1): 26–34

Wang Peigao, Liu Zongyi, Zhang Kaidou. 2004. Applied Satellite Meteorology (in Chinese). Qingdao: Ocean University of China Press, 232–234

Woodruff S D, Slutz R J, Jenne R L, et al. 1987. A comprehensive ocean-atmosphere data set. Bull Amer Meteor Soc, 68(10): 1239–1250

Worley S J, Woodruff S D, Reynolds R W, et al. 2005. I_COADS release 2.1 data and products. Int J Climatol, 25(7): 823–842

Yan Junyue, Chen Qianjin, Zhang Xiuzhi. 1993. Marine Climate in the Adjacent Seas of China (in Chinese). Beijing: Science Press, 279–280

Zhang Suping, Ren Zhaopeng. 2010. The influence of the thermal effect of underlaying surface on the spring sea fog over the Huanghai Sea: observations and numerical simulations. Acta Meteor Sin (in Chinese), 68(4): 439–449

Zhang Suping, Xie Shangping, Liu Qinyu, et al. 2009. Seasonal variations of Huanghai Sea fog: observations and mechanisms. J Climate, 22(24): 6758–6772

Zhao Yongping, Chen Yongli, Wang Pigao. 1997. Analysis of atmospheric and oceanic conditions for marine fog formation over the Huanghai Sea and East China Sea. Stud Mar Sin (in Chinese), (38): 69–77

Zhou Faxiu, Liu Longtai. 1986. The report of comprehensive investigation for the adjacent seas of the mouth of Changjiang River and Jeju Island: sea fog. Journal of Shandong College of Oceanology (in Chinese), 16(1): 115–131

Zhou Faxiu, Wang Xin, Bao Xianwen. 2004. Climatic characteristics of sea fog formation of the Huanghai Sea in spring. Haiyang Xuebao (in Chinese), 26(3): 28–37